Supporting Information

Two "X"-shaped {Eu_6}-embedded water-soluble heterometallic polyoxotungstates based on {$Eu_6M_4WSe_4(GeW_{10})_4$} (M = Cr, Al) clusters with resistance-switching

Yun-Fei Cao, Ju-Ning Chen, Xiao-Min Shen, Yan-Qiong Sun,* Shou-Tian Zheng*

Fujian Provincial Key Laboratory of Advanced Inorganic Oxygenated-Materials, College of Chemistry, Fuzhou University, Fuzhou, Fujian 350108, China.

This file includes:

Section 1: Experimental Methods

Materials and Instrumentation. Ethylenediamine (en), $Eu(NO_3)_3·6H_2O$, $KCr(SO_4)_2$, Na_2SeO_3, $K_2C_2O_4$ were commercially purchased without further purification. $K_8Na_2[A\text{-}\alpha\text{-}GeW_9O_{34}]·25H_2O$ was synthesized according to the reported procedure [1]. PXRD patterns were obtained by using an Ultima IV diffractometer with Cu-*Kα* radiation (λ = 1.5418 Å) in the range 3 - 45°. Inductively coupled plasma (ICP) spectrometer analyses were conducted on an Ultima2 spectrometer. Thermal analysis was performed in a dynamic air atmosphere with a heating rate of 10 °C/min, using a NETZSCH STA 449C thermal analyzer. IR spectra were determined in the range 4000-500 cm^{-1} on a Nicolet IS50 Fourier transform infrared (FT/IR) spectrometer. The optical diffuse reflectance spectra were measured at room temperature using a Perkin-Elmer Lambda 900 UV-vis spectrophotometer equipped with an integrating sphere attachment and $BaSO_4$ as reference. Luminescent spectra were collected with an Edinburgh Instruments FS980 TCSPC luminescence spectrometer on powdered crystal material of the compounds.

Synthesis of 1-EuCr: A mixture of $K_8Na_2[A\text{-}\alpha\text{-}GeW_9O_{34}]·25H_2O$ (0.513 g, 0.202 mmol), $Eu(NO_3)_3·6H_2O$ (0.075 g, 0.168 mmol)，$K_2C_2O_4$ (0.102 g, 0.553 mmol) , Na_2SeO_3 (0.053 g, 0.318 mmol), $KCr(SO_4)_2$ (0.051 g, 0.102 mmol) and 5 mL of H_2O was stirred for 5 minutes in a 23 mL Teflon-lined autoclave, then 150 μL of en was added, successively. The mixture was stirred for 1 hour and then heated at 100 ℃ for 3 days. After cooling to room temperature and washing with mother solution, greenish plate crystals were obtained. The initial pH of the reaction mixture before heating was 7.6, which decrease to 6.8 after cooling. Yield: 40 mg (11% based on Eu). IR for **1-EuCr**: 3394 cm^{-1} (s), 1623 cm^{-1} (m), 1467 cm^{-1} (w), 1363 cm^{-1} (w), 939 cm^{-1} (m), 862 cm^{-1} (w), 786 cm^{-1} (s), 725 cm^{-1} (s), 657 cm^{-1} (s), 609 cm^{-1} (s).

Synthesis of 2-EuAl: The preparation process of **2-EuAl** is identical to **1-EuCr** except that $KCr(SO_4)_2$ was replaced by $KAl(SO_4)_2$. Colorless plate crystals were obtained. The initial pH of the reaction mixture before heating was 7.8, and dropped to 7.2 after cooling. Yield: 55 mg (15% based on Eu). IR for **2-EuAl**: 3073 cm^{-1} (s), 1629 cm^{-1} (m), 1465 cm^{-1} (w), 1024 cm^{-1} (w), 939 cm^{-1} (m), 773 cm^{-1} (s), 732 cm^{-1} (s), 595 cm^{-1} (s).

Single–crystal X–ray diffraction: Crystals were collected on a Bruker D8 Venture CCD area diffractometer equipped with a fine focus 2.0 kW sealed tube X-ray source (MoKα radiation, λ = 0.71073 Å) operating at 170 (2) K. The empirical absorption correction was based on equivalent reflections. Structures were solved by direct methods followed by successive difference Fourier methods. Computations were performed using SHELXTL-2018/3 and final full-matrix refinements were against F^2. The contribution of disordered solvent molecules to the overall intensity data of structures was treated using the SQUEEZE method in PLATON. CCDC 2521983 (**1-EuCr)** and 2521982 (**2-EuAl**) contains the crystallographic data.

The electrical bistability measurements

During the electrical bistability test, the current was limited to 0.5 A. The positive terminal was connected to the Ag electrode, while the negative terminal was connected to the ITO conductive glass, with a voltage scanning rate of 5 $V·S^{-1}$.

Pretreatment of conductive glass

A 400 nm ITO conductive glass (20 × 20 mm) was pre-cleaned using ultrapure water, acetone,

ethanol, and isopropanol for 15 minutes in each solvent, and then the substrates were dried in an oven for subsequent use.

Fabrication of memory devices

Spin coating method was used in the fabrications of the memory devices. The crystal samples **1-EuCr** or **2-EuAl** are soluble in water. The aqueous solution containing sample powder was spin-coated onto the substrate, first at a low speed of 500 rpm for 10 seconds, and then at a high speed of 2000 rpm for 30 seconds. The active layer was annealed at 60 ºC in an oven for 2 h. Afterward, the top electrodes were prepared by sprinkling the turbid liquid of Ag nanowires (0.5 mg·mL^{-1}) for 1 h through a shadow mask with circular holes with a diameter of about 0.1 cm. Finally, the devices were further dried at 60 ºC for 1 h to improve their adhesive force. In the device endurance testing, an interval of 10 min was adopted to equilibrate the system.

The conductivity measurements

Separately, 10 mg of the sample was weighed and placed into the mold of a tablet press. A certain pressure was applied to compact the sample into a square pellet with a cross-section of 2 mm × 2 mm. Silver wires were bonded to both ends of the sample with silver paste, and a conductive pen was used to enhance the electrical connection at the two terminals. All electrical measurements were performed on a Keithley 2636B dual-channel source meter. The resistivity was calculated according to the equation $\rho = \frac{L}{RS}$, and all relevant graphs were plotted using Origin software.

The topology analysis

The TOPOS software is used to analyze the topology of **1-EuCr**. Topologically, the 3D framework of **1-EuCr** adopts a 6-connected *pcu* topology. Each $\{Eu_6Cr_4WSe_4(GeW_{10})_4\}$ polyanion serves as a 6-connected node and the K^+ / Na^+ cations function as linkers. The Schäfli symbol is $(4^{12}.6^3)$ and the shortest closed loop around the the nodes are twelve 4-circuits and three 6-circuits.

The topology analysis is provided as follows:

Topology for Eu1

Atom Eu1 links by bridge ligands and has

Common vertex with					R(A-A)	
Eu 1	-0.1181	1.2272	-0.1251	(0 2 0)	16.910A	1
Eu 1	0.1181	0.7272	0.6251	(0 1 0)	17.896A	1
Eu 1	0.1181	0.7272	-0.3749	(0 1-1)	17.896A	1
Eu 1	-0.1181	0.2272	-0.1251	(0 1 0)	19.068A	1
Eu 1	0.8819	1.2728	0.3749	(1 0 0)	25.395A	1
Eu 1	0.8819	0.2728	0.3749	(1-1 0)	25.395A	1

Structural group analysis

Structural group No 1

Structure consists of 3D framework with Eu

Coordination sequences

Eu1: 1 2 3 4 5 6 7 8 9 10
Num 6 18 38 66 102 146 198 258 326 402
Cum 7 25 63 129 231 377 575 833 1159 1561

TD10=1561
Vertex symbols for selected sublattice

Eu1 Point symbol:{4^12.6^3}
Extended point symbol:[4.4.4.4.4.4.4.4.4.4.4.6(4).6(4).6(4)]

Point symbol for net: {4^12.6^3}
6-c net; uninodal net
Topological type: pcu alpha-Po primitive cubic; 6/4/c1; sqc1 (topos&RCSR.ttd) {4^12.6^3} - VS [4.4.4.4.4.4.4.4.4.4.4.*.*.*] (72442 types in 11 databases)

Section 2: Additional Tables

Table S1. Crystal data and structure refinement for 1-EuCr and 2-EuAl

Compound	**1-EuCr**	**2-EuAl**
Empirical formula	$H_{17}Na_4K_7(H_2O)_{12}[Eu_6(H_2O)_4Cr_4(WO_6)(SeO_3)_4(GeW_{10}O_{37})_2(GeW_{10}O_{38})_2]\cdot 32H_2O$	$H_{17}Na_2K_9(H_2O)_{14}[Eu_6(H_2O)_4Al_4(WO_6)(SeO_3)_4(GeW_{10}O_{37})_2(GeW_{10}O_{38})_2]\cdot 32H_2O$
Formula weight	13199.32	13163.48
Temperature/K	170	170
Crystal system	monoclinic	monoclinic
Space group	$P2_1/c$ (14)	$P2_1/c$
a/Å	25.084(3)	24.765(4)
b/Å	29.165(3)	29.023(5)
c/Å	35.693(4)	35.461(6)
α/°	90	90
β/°	92.410(2)	91.971(3)
γ/°	90	90
Volume/Å^3	26089(5)	25473(7)
Z	4	4
ρ_{calc} g/cm^3	3.246	3.340
μ/mm^{-1}	20.782	21.169
F(000)	22036	22179
2θ range for data collection/°	3.02 to 50.04	3.11 to 50.10
Reflections collected	130704	125703
Independent reflections	45617 [R_{int} = 0.0636, R_{sigma} = 0.0755]	44547 [R_{int} = 0.0655, R_{sigma} = 0.0786]
Data/restraints/parameters	45617 / 138 / 2316	44547 / 192 / 2425
Data completeness	99.0%	98.7%
Goodness-of-fit on F^2	1.054	1.034
Final *R* indexes [I>=2σ (I)]	R_1 = 0.0522, wR_2 = 0.1191	R_1 = 0.0558, wR_2 = 0.1373
Final *R* indexes [all data]	R_1 = 0.0848, wR_2 = 0.1324	R_1 = 0.0894, wR_2 = 0.1553

[a]$R_1 = \sum||F_o|-|F_c||/\sum|F_o|$, [b]$\omega R_2 = \{\sum\omega[(F_o)^2-(F_c)^2]^2/\sum\omega[(F_o)_2]^2\}^{1/2}$

Table S2. Inductively coupled plasma spectroscopy (ICP) analysis of 1-EuCr

	Atom name	W	Eu	Se	Ge	Cr
	Calculated (%)	57.10	6.90	2.39	2.20	1.57
1-EuCr	**Found (%)**	57.43	6.76	2.23	1.12	1.43

Table S3. Inductively coupled plasma spectroscopy (ICP) analysis of 2-EuAl

	Atom name	W	Eu	Se	Ge	Al
	Calculated (%)	57.40	6.94	2.40	2.21	0.82
2-EuAl	**Found (%)**	57.56	6.88	2.34	2.16	0.72

Table S4. Bond valence sum (BVS) calculations of all Cr and Se atoms in 1-EuCr

	Atom name	BVS	Oxidation state
	Cr1	3.055	Cr^{3+}
1-EuCr	**Cr2**	3.069	Cr^{3+}
	Cr3	2.980	Cr^{3+}
	Cr4	3.075	Cr^{3+}
	Se1	3.74	Se^{4+}
	Se2	3.71	Se^{4+}
	Se3	3.70	Se^{4+}
	Se4	3.71	Se^{4+}

Table S5. Bond valence sum (BVS) calculations of all Al and Se atoms in 2-EuAl

	Atom name	BVS	Oxidation state
	Al 1	3.025	Al^{3+}
2-EuAl	**Al 2**	3.020	Al^{3+}
	Al 3	3.14	Al^{3+}
	Al 4	3.13	Al^{3+}
	Se 1	3.69	Se^{4+}
	Se 2	3.67	Se^{4+}
	Se 3	3.69	Se^{4+}
	Se 4	3.68	Se^{4+}

Table S6. The electrical conductivity and electrical bistability property of 1-EuCr and 2-EuAl

	1-EuCr	2-EuAl
V_{set} (V)	3.92	1.12
V_{reset} (V)	−7.61	−7.34
I_{ON}/I_{OFF}	1.73×10^4	1.57×10^3
ρ (S/m)	5.88×10^{-4}	2.14×10^{-3}

Table S7. The m/z assignment of 1-EuCr

	m/z(calc)	m/z(obs)	Assignment
8–	1525.8496	1525.8353	$\{H_{14}K_2Na_4Eu_6Cr_4Se_4Ge_4W_{41}O_{168}(4H_2O)\}^{8-}$
7–	1759.7079	1759.6479	$\{H_{14}K_3Na_4Eu_6Cr_4Se_4Ge_4W_{41}O_{168}(8H_2O)\}^{7-}$
6–	2069.2031	2069.4052	$\{H_{12}K_6Na_4Eu_6Cr_4Se_4Ge_4W_{41}O_{168}(7H_2O)\}^{6-}$
5–	2494.4664	2494.2739	$\{H_{12}K_7Na_4Eu_6Cr_4Se_4Ge_4W_{41}O_{168}(8H_2O)\}^{5-}$

Table S8. The m/z assignment of 2-EuAl

	m/z(calc)	m/z(obs)	Assignment
6–	2032.1849	2032.2847	$\{H_{16}K_5Na_1Eu_6Al_4Se_4Ge_4W_{41}O_{168}(6H_2O)\}^{6-}$
5–	2450.4258	2450.3489	$\{H_{16}K_5Na_2Eu_6Al_4Se_4Ge_4W_{41}O_{168}(8H_2O)\}^{5-}$
4–	3095.3258	3095.2129	$\{H_{16}K_6Na_2Eu_6Al_4Se_4Ge_4W_{41}O_{168}(13H_2O)\}^{4-}$

Table S9. The m/z assignment of 1-EuCr in the pH = 3.4

	m/z(calc)	m/z(obs)	Assignment
5–	2497.8040	2497.7554	$\{H_{12}K_7Na_4Eu_6Cr_4Se_4Ge_4W_{41}O_{168}(9H_2O)\}^{5-}$
4–	3148.9629	3148.9629	$\{H_{14}K_7Na_3Eu_6Cr_4Se_4Ge_4W_{41}O_{168}(16H_2O)\}^{4-}$

Table S10. The m/z assignment of 1-EuCr in the pH = 10.2

	m/z(calc)	m/z(obs)	Assignment
5–	2502.0816	2502.9102	$\{H_{11}K_8Na_4Eu_6Cr_4Se_4Ge_4W_{41}O_{168}(8H_2O)\}^{5-}$
4–	3219.8443	3219.6310	$\{H_{15}K_7Na_2Eu_6Cr_4Se_4Ge_4W_{41}O_{168}(13H_2O)\}^{4-}$
4–	3144.3558	3144.8774	$\{H_{14}K_7Na_3Eu_6Cr_4Se_4Ge_4W_{41}O_{168}(15H_2O)\}^{4-}$

Table S11. The m/z assignment of 2-EuAl in the pH = 3.4

	m/z(calc)	m/z(obs)	Assignment
5–	2481.0621	2481.3994	$\{H_{12}K_9Na_2Eu_6Al_4Se_4Ge_4W_{41}O_{168}(8H_2O)\}^{5-}$
4–	3123.1097	3122.9923	$\{H_{14}K_9Na_1Eu_6Al_4Se_4Ge_4W_{41}O_{168}(14H_2O)\}^{4-}$

Table S12. The m/z assignment of 2-EuAl in the pH = 10.2

	m/z(calc)	m/z(obs)	Assignment
5–	2495.2911	2495.7327	$\{H_{12}K_9Na_2Eu_6Al_4Se_4Ge_4W_{41}O_{168}(12H_2O)\}^{5-}$
5–	2483.6897	2483.5434	$\{H_{13}K_9Na_1Eu_6Al_4Se_4Ge_4W_{41}O_{168}(10H_2O)\}^{5-}$
5–	2472.8794	2472.1280	$\{H_{13}K_9Na_1Eu_6Al_4Se_4Ge_4W_{41}O_{168}(7H_2O)\}^{5-}$
4–	3132.8793	3133.4243	$\{H_{13}K_9Na_2Eu_6Al_4Se_4Ge_4W_{41}O_{168}(15H_2O)\}^{4-}$
4–	3118.3801	3118.1744	$\{H_{14}K_9Na_1Eu_6Al_4Se_4Ge_4W_{41}O_{168}(13H_2O)\}^{4-}$
4–	3104.8793	3104.6689	$\{H_{14}K_9Na_1Eu_6Al_4Se_4Ge_4W_{41}O_{168}(10H_2O)\}^{4-}$
4–	3089.8467	3089.4024	$\{H_{16}K_8Eu_6Al_4Se_4Ge_4W_{41}O_{168}(10H_2O)\}^{4-}$

Table S13. The solvent solubility of compound **1-EuCr** in various common solvents

Solvent	Solubility	Solvent	Solubility
Methanol	Soluble	carbon tetrachloride	Insoluble
ethanol	Soluble	dichloromethane	Insoluble
1-Butanol	Soluble	DMSO	Insoluble
Cyclohexane	Insoluble	DMF	Insoluble

The solubility of compound **1-EuCr** is 6.8 mg/mL, while that of compound **2-EuAl** is 8.0 mg/mL at room temperature. Furthermore, the solvent solubility of compound **1-EuCr** in various common solvents was systematically investigated, and the results are summarized in Table S13.

Section 3: Additional Figs

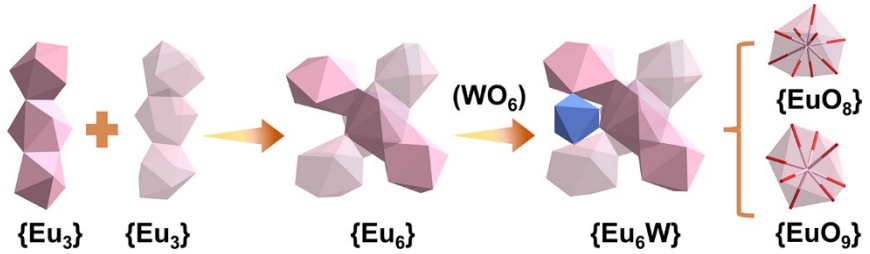

Fig. S1 The assembly of $\{Eu_6\}$ cluster and the coordination environment of Eu^{3+} in **1-EuCr**.

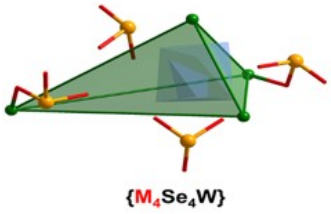

Fig. S2 Schematic view of $\{M_4Se_4W\}$ (M = Cr) cluster in **1-EuCr**.

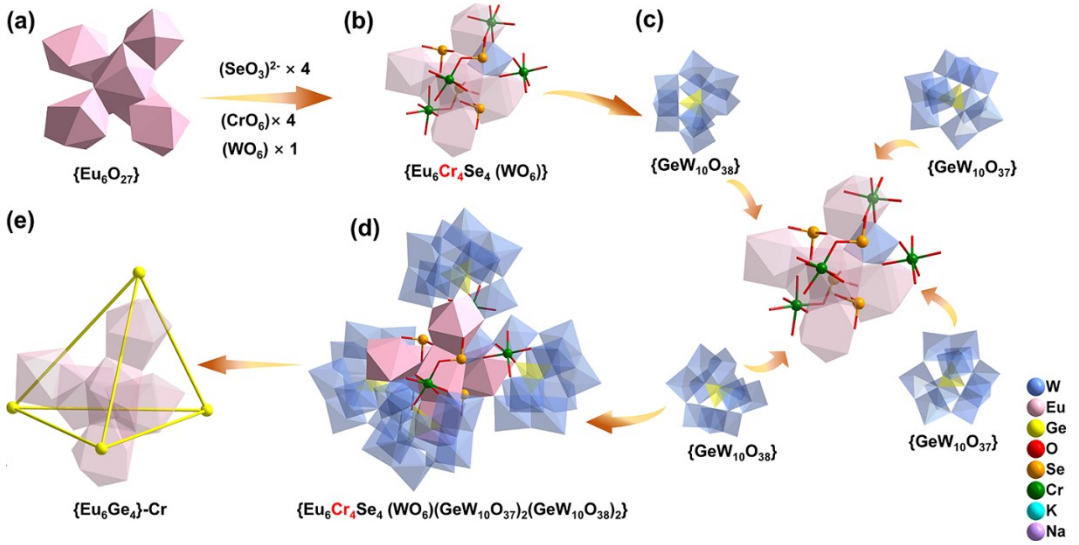

Fig. S3 View of the construction of $\{\mathbf{Eu_6Cr_4WSe_4(GeW_{10})_4}\}$ cluster in **1-EuCr**: (a) $\{Eu_6\}$ cluster, (b) $\{Eu_6Cr_4Se_4(WO_6)\}$ cluster, (c)-(d) the $\{\mathbf{Eu_6Cr_4WSe_4(GeW_{10})_4}\}$ constructed from $\{Eu_6Cr_4Se_4(WO_6)\}$ cluster and two $[GeW_{10}O_{37}]^{10-}$and two $[GeW_{10}O_{38}]^{12-}$ clusters, (e) the simplified structure diagram of $\{\mathbf{Eu_6Cr_4WSe_4(GeW_{10})_4}\}$.

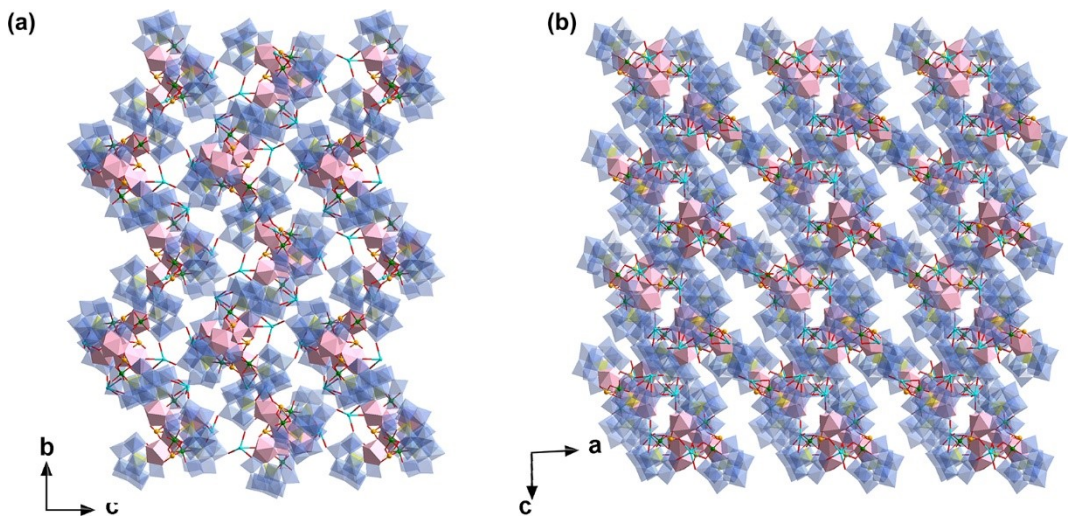

Fig. S4 (a) View of the 2D layer in *bc* plane of **1-EuCr** (b) along the *b* axis.

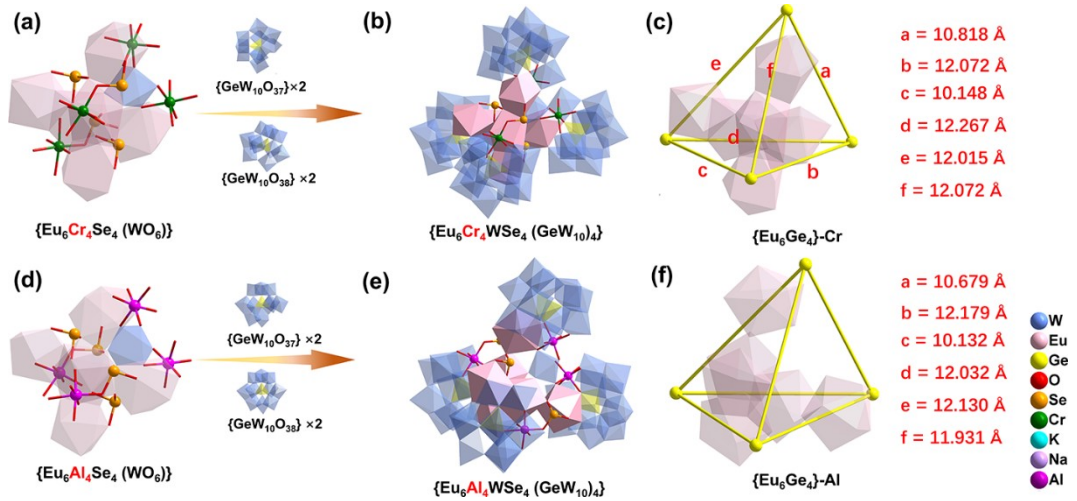

Fig. S5 (a-b) View of the assembly of {$\mathbf{Eu_6Cr_4Se_4Ge_4W_{41}}$} in **1-EuCr**; (d-e) view of the assembly of {$\mathbf{Eu_6Al_4Se_4Ge_4W_{41}}$} in **2-EuAl**; (c, f) simplified structure diagram of **1-EuCr** and **2-EuAl**.

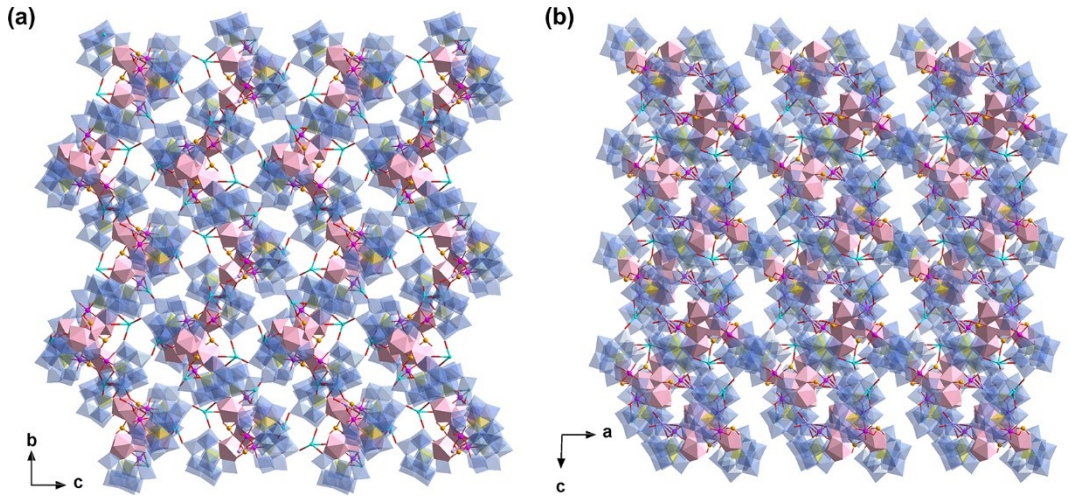

Fig. S6 (a) View of the 2D layer in **2-EuAl** in the *bc* plane; (b) view of the 3D framework of **2-EuAl** along the *b* axis.

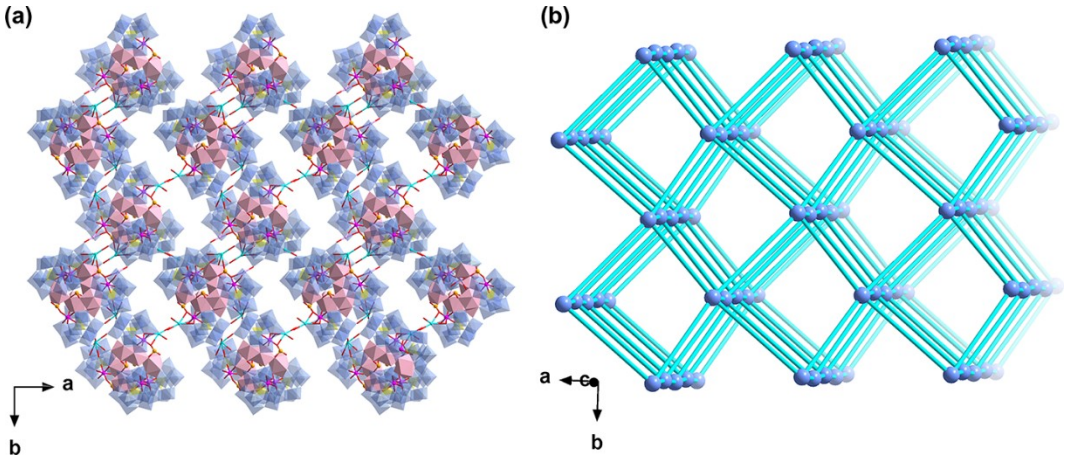

Fig. S7 (a) View of the 3D framework of **2-EuAl** along the *c* axis; (b) schematic view of *pcu*-type net of **2-EuAl**.

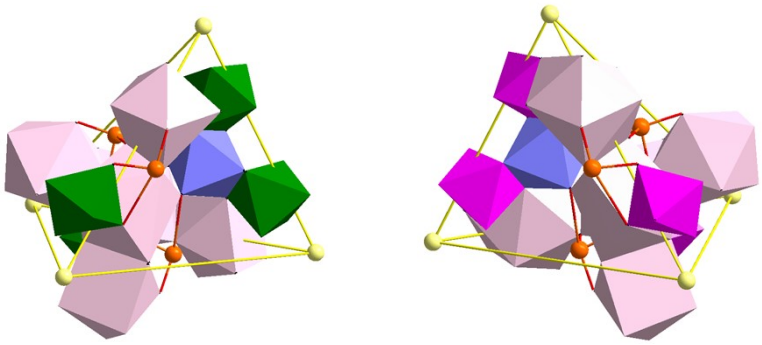

{Eu$_6$Cr$_4$Se$_4$Ge$_4$W$_{41}$} **{Eu$_6$Al$_4$Se$_4$Ge$_4$W$_{41}$}**

Fig. S8 Schematic view of the **{Eu$_6$Cr$_4$Se$_4$Ge$_4$W$_{41}$}** cluster in **1-EuCr** and **{Eu$_6$Al$_4$Se$_4$Ge$_4$W$_{41}$}** in **2-EuAl**. Color code: $EuO_{8/9}$ polyhedrons, pink; CrO_6 octahedron, green; WO_6 octahedron, blue; {GeW_{10}} cluster, yellow nodes; Se, orange; O, red.

Section 4: Additional Characterizations

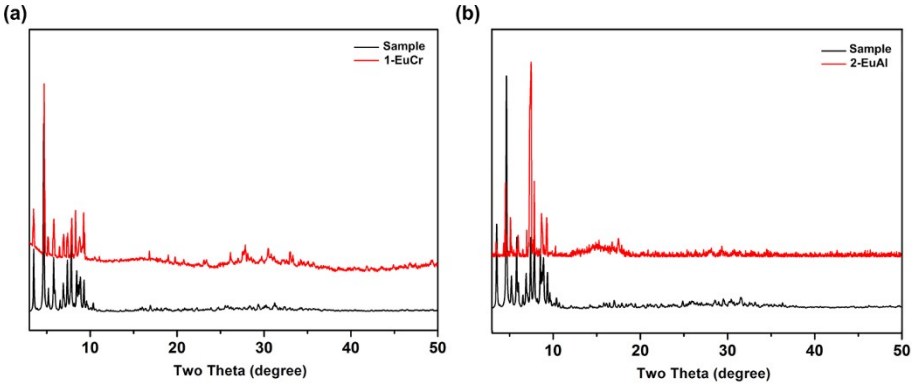

Fig. S9 Simulated and experimental PXRD patterns of **1-EuCr** (a) and **2-EuAl** (b).

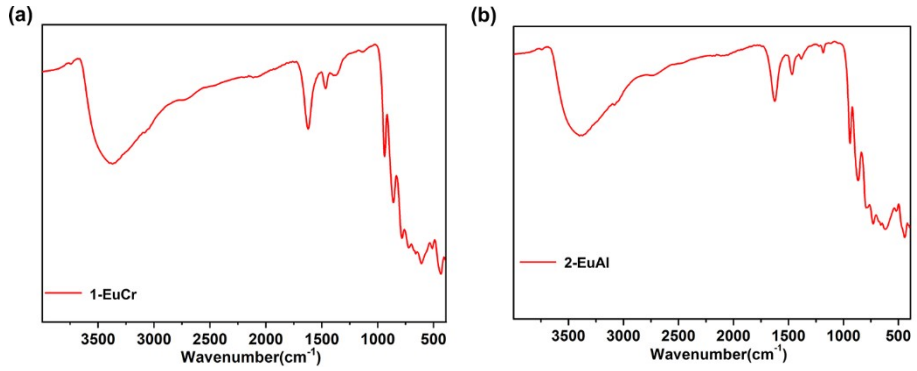

Fig. S10 FT-IR spectra of **1-EuCr** (a) and **2-EuAl** (b).

The IR spectra of compounds **1-EuCr** and **2-EuAl** show that the wide peak around 3500 - 2800 cm^{-1} is assigned to the stretching vibration of the O-H groups of water molecules, while the peak at ca. 1630 cm^{-1} corresponds to the H O H bending vibration of coordinated water molecules. The strong peaks in the range of 1000−900 cm^{-1} are attributed to the asymmetric stretching vibrations of terminal W=O bonds (ν_{as}(W=O_t)). The peaks at 900-800 cm^{-1} region are ascribed to Ge-O stretching vibration, while those at the 800-700 cm^{-1} are attributed to the asymmetric stretching vibrations of bridging W–O_b–W and W–O_c–W. The Cr−O / Al-O and Ln−O stretching vibration peaks appear at about 516 cm^{-1}, 439 cm^{-1}, respectively. (O_t: terminal oxygen, O_b: bridging oxygen, O_c: central oxygen).

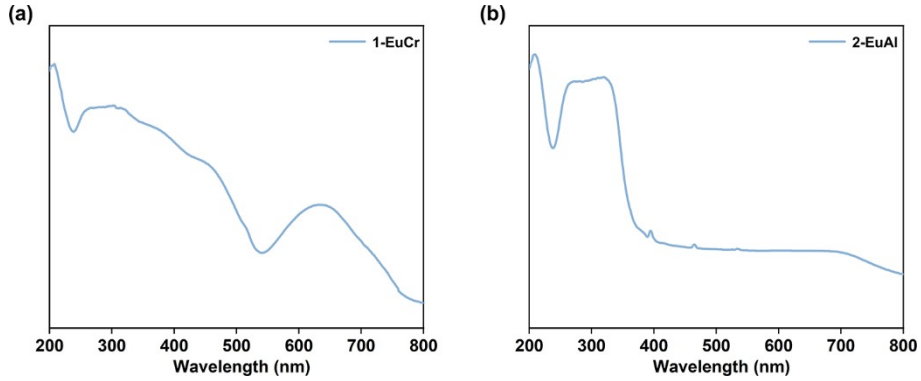

Fig. S11 The solid-state UV-vis absorption spectra of **1-EuAl (a)** and **2-EuAl (b)**.

The UV-Vis absorption spectrum of **1-EuCr** exhibits characteristic bands corresponding to both the polyoxometalate framework and the incorporated Cr^{3+} metal centers. The intense absorption bands 200 - 320 nm are assigned to ligand-to-metal charge transfer (LMCT) transitions, originating from the O → W and Ge → O transition within the tungstogermanate framework. The broad absorption bands in the 350–700 nm range are attributed to spin-allowed d-d transitions of the octahedrally coordinated Cr^{3+} centers ($^4A_{2g} \rightarrow {}^4T_{1g}$ and $^4A_{2g} \rightarrow {}^4T_{2g}$).

The UV-Vis absorption spectrum of **2-EuAl** exhibits characteristic bands corresponding to the polyoxometalate framework. The intense absorption bands 200 - 350 nm are assigned to ligand-to-metal charge transfer (LMCT) transitions, originating from the O → W and Ge → O transition within the tungstogermanate framework. In contrast to **1-EuCr**, no obvious d-d absorption bands are observed in the visible region (400–800 nm), which is consistent with the d^0 configuration of Al^{3+} centers.

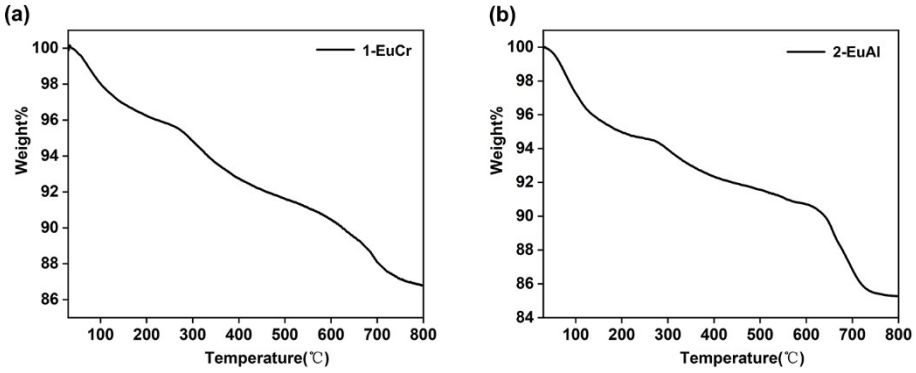

Fig. S12 TGA curve of **1-EuCr** and **2-EuAl**.

The thermogravimetric analyses of **1-EuCr** and **2-EuAl** were performed under an air-flow atmosphere over the temperature range of 30-800 ℃ at the heating rate of 10 ℃/min. For **1-EuCr**, the weight loss of 4.30% from 30 ℃ to 150 °C is attributed to the loss of 32 free water molecules per formula unit (calc. 4.36%). After 600 °C, **1-Eu** starts to decompose. For **2-EuAl**, the weight loss of 4.30% from 30 °C to 152 °C corresponds to the release of 32 free water molecules per formula unit (calc. 3.89%). After 600 °C, **2-EuAl** starts to decompose.

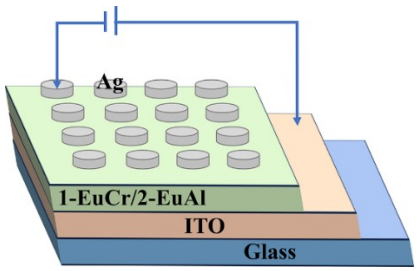

Fig S13. The 3D schematic illustration of the device.

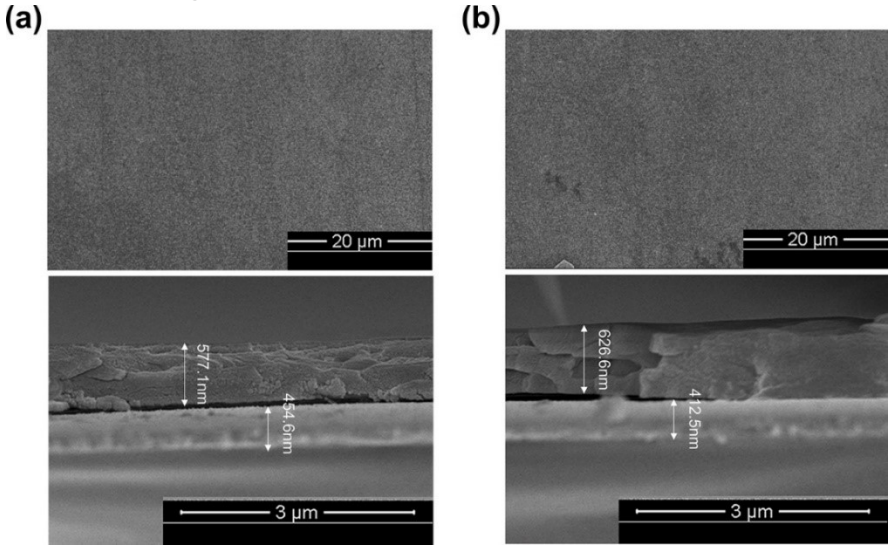

Fig. S14 (a) Surface morphology and cross section of **1-EuCr** film; (b) Surface morphology and cross section of **2-EuAl** film.

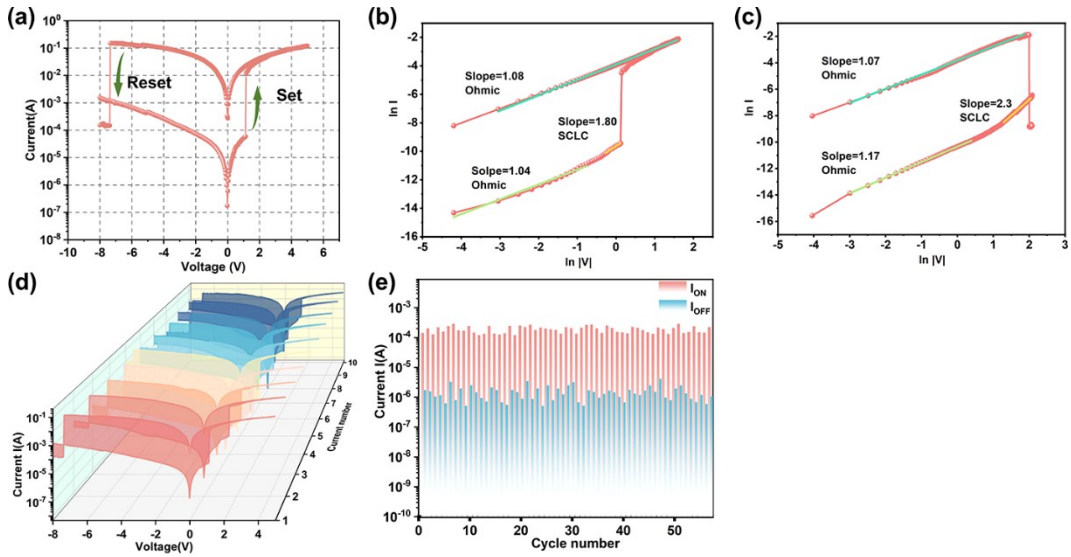

Fig. S15 Resistive switching (RS) characteristics of ITO/**2-EuAl** (3 mg mL^{-1})/Ag memristor at room temperature: (a) typical current–voltage (*I–V*) characteristics showing the OFF-to-ON transitions; (b) logI–log|V| curves with the fitted conduction mechanism under positive voltage sweep and (c) negative voltage sweep; (d) typical *I–V* curves showing 10 cycles; (e) stability showing the currents of low resistance state (LRS) and high resistance state (HRS) with 58 cycles of **2-EuCr**.

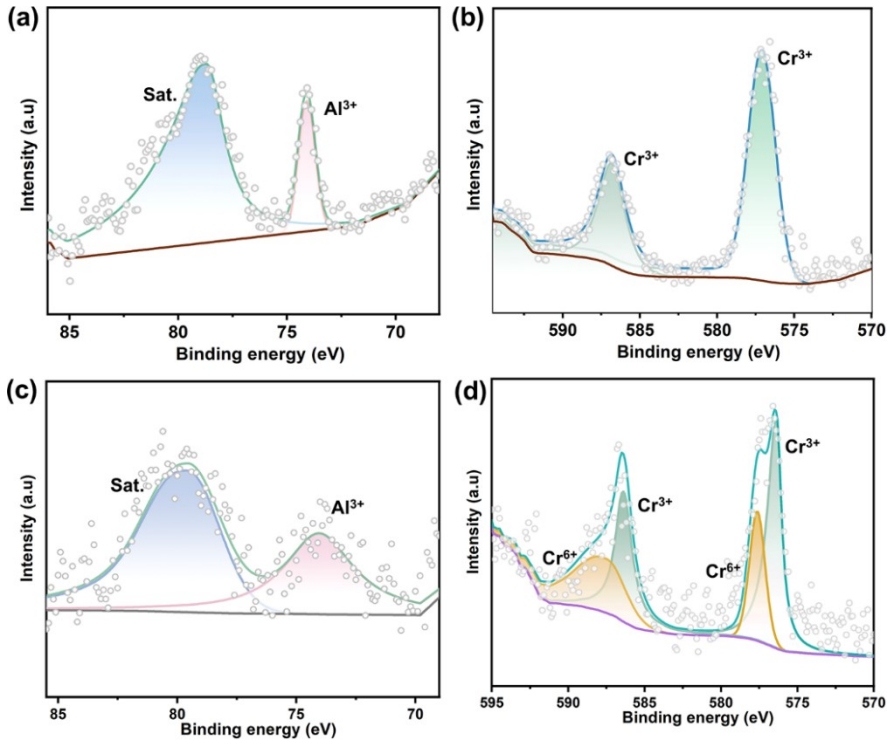

Fig. S16 XPS spectra of **2-EuAl** for Al atoms before (a) and after (c) applying bias voltage; XPS spectra of **1-EuCr** for Cr atoms before(b) and after (d) applying bias voltage.

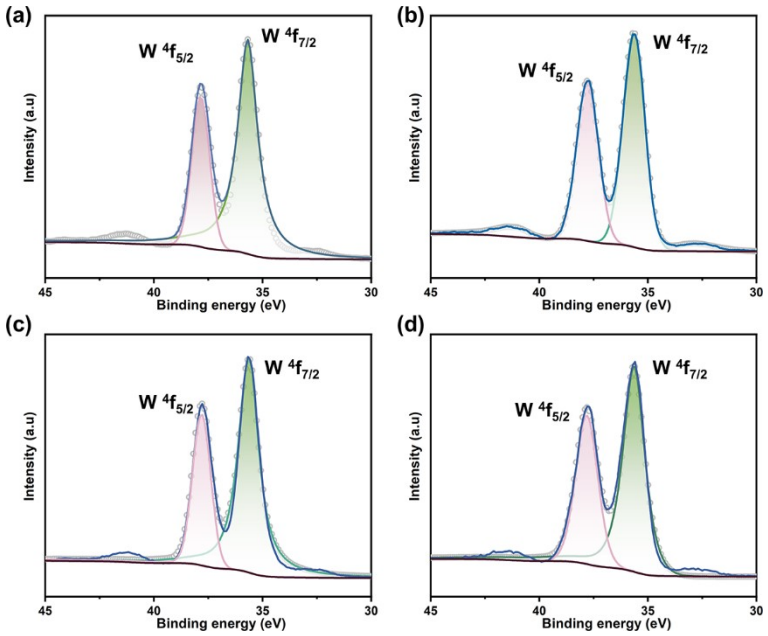

Fig. S17. XPS spectra of **1-EuCr** for W atoms before (a) and after (c) applying bias voltage; XPS spectra of **2-EuAl** for W atoms before (b) and after (d) applying bias voltage.

As shown in the Fig S20, the characteristic peaks observed in the high-resolution W 4f spectrum originate from spin-orbit coupling. Two distinct peaks are observed at approximately 35.6 eV and 37.7 eV, assigned to the W $4f_{7/2}$ and W $4f_{5/2}$ orbitals, respectively. These binding energy values are consistent with the W^{6+} in the polyoxotungstate cluster. Therefore, the oxidation states of the W atoms in the compounds **1-EuCr** and **2-EuAl** remain unchanged before and after applying bias voltage.

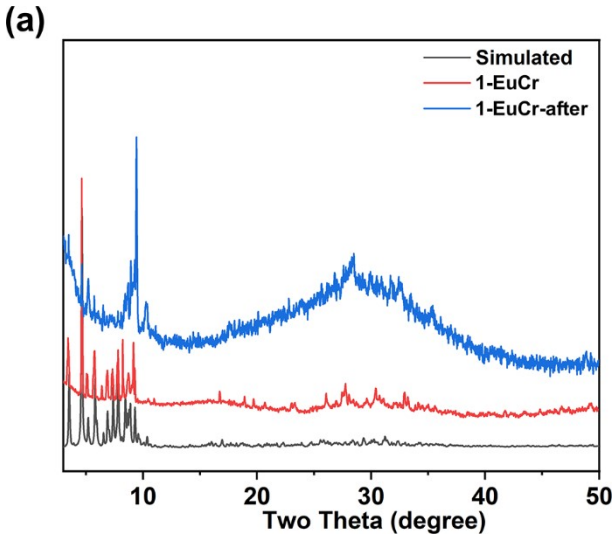

Fig S18. Simulated and experimental PXRD patterns of **1-EuCr** before and after applying a positive bias voltage.

The overall structure of the Cr-contained framework indeed undergo structural change with the oxidation of Cr^{3+} to Cr^{6+} after applying a positive bias voltage. The XRD results showed that the diffraction peaks of the sample after applying a positive bias voltage cannot fully match the simulated pattern, indicating that the occurrence of partial structural transformation. Nevertheless, the precise structure after the altered phase cannot be identified by single-crystal diffraction.

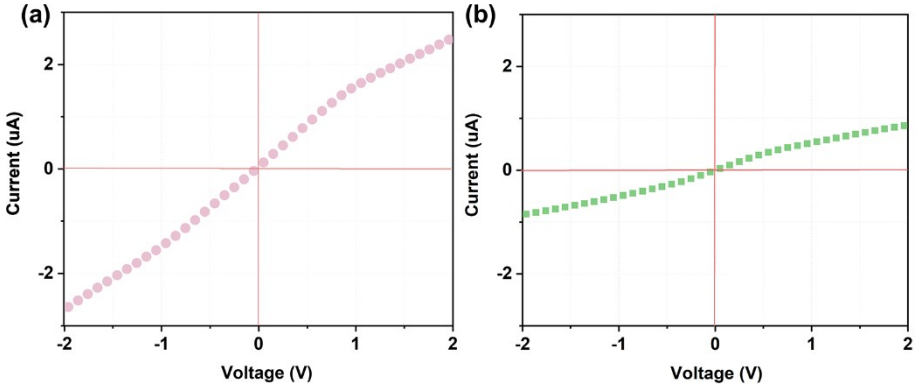

Fig. S19 The electrical conductivity of **2-EuAl**(a) and **1-EuCr** (b).

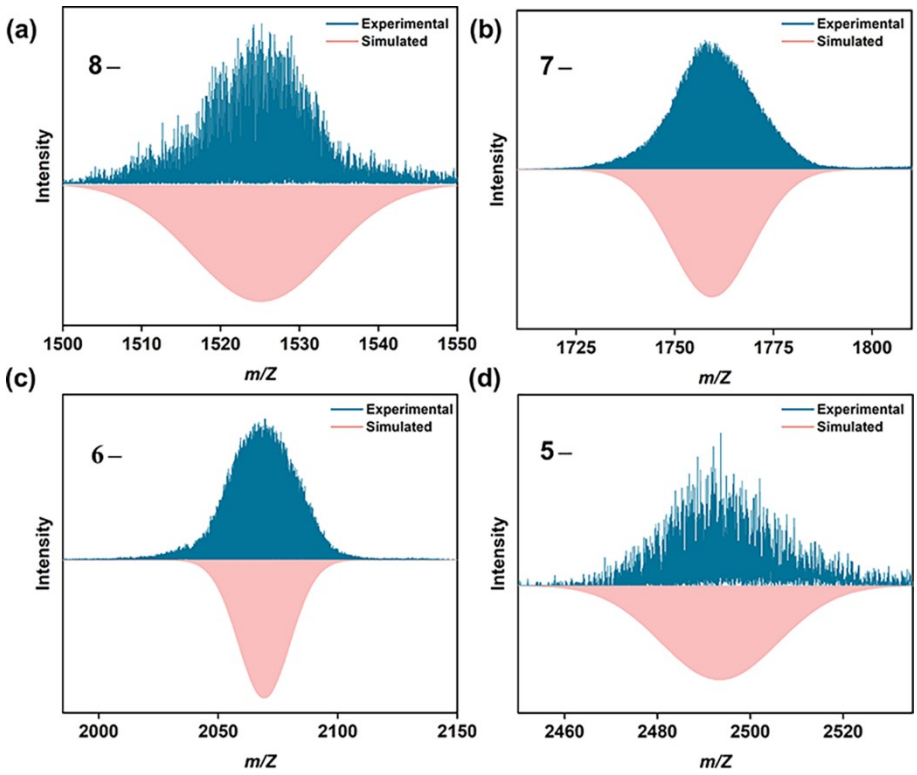

Fig. S20 Experimental (upper, blue) and simulative (under, pink) peaks of the ESI-MS spectra for **1-EuCr**.

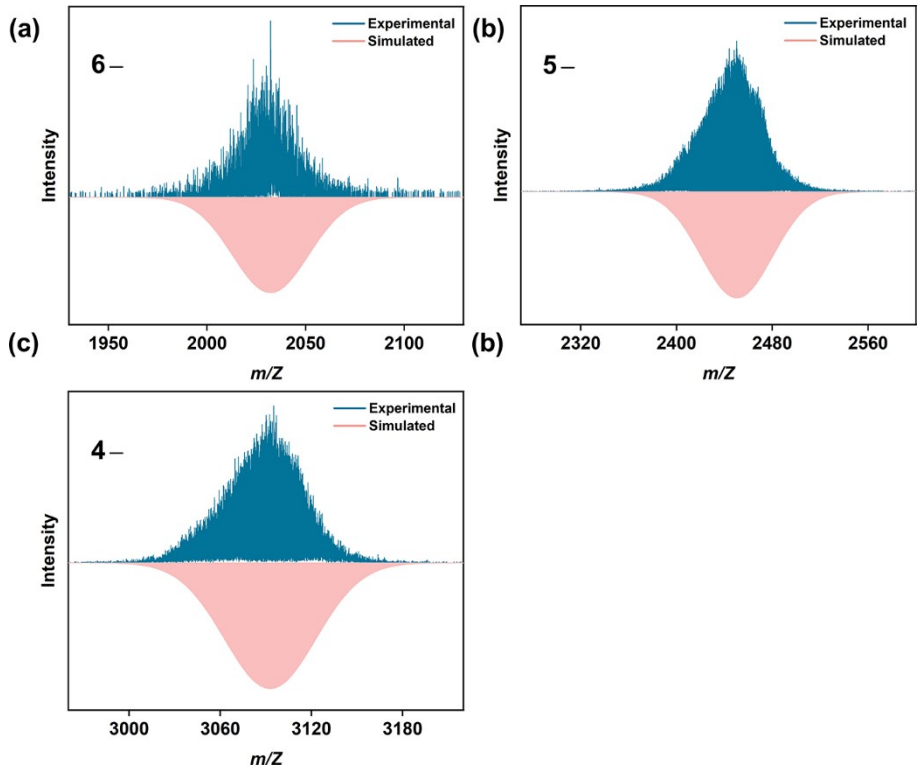

Fig. S21 Experimental (upper, blue) and simulative (under, pink) peaks of the ESI-MS spectra for **2-EuAl**.

In Fig. S17 and S18, the negative mode of full scan mass spectra of the **1-EuCr** and **2-EuAl** have been provided. The spectrum shows four dominant peaks for 8−, 7−, 6− and 5− charged ions, attributed to the intact cluster $\{H_{14}K_2Na_4Eu_6Cr_4Se_4Ge_4W_{41}O_{168}(4H_2O)\}^{8-}$, $\{H_{14}K_3Na_4Eu_6Cr_4Se_4Ge_4W_{41}O_{168}(8H_2O)\}^{7-}$, $\{H_{12}K_6Na_4Se_4Eu_6Cr_4Se_4Ge_4W_{41}O_{168}(7H_2O)\}^{6-}$ and $\{H_{12}K_7Na_4Eu_6Cr_4Se_4Ge_4W_{41}O_{168}(8H_2O)\}^{5-}$ of compound **1-EuCr**, respectively (Fig. S16). Prominent peaks that appear at m/z 1525.8353 (simulated 1525.8496), 1759.6479 (simulated 1759.7079), 2069.4052 (simulated 2069.2031), and 2494.2739 (simulated 2494.4664) clearly proves the stability of the complete $\{\mathbf{Eu_6Cr_4Se_4Ge_4W_{41}}\}$ cluster of **1-EuCr** in aqueous. Meanwhile, the ESI-MS spectrum displays three prominent envelopes consistent with the complete group for **2-EuAl** (Fig. S17). These peaks were appointed to charge in 6−, 5− and 4− at m/z of 2032.2847 $\{H_{16}K_5Na_1Eu_6Al_4Se_4Ge_4W_{41}O_{168}(6H_2O)\}^{6-}$ (simulated 2032.1849), 2450.3489, $\{H_{16}K_5Na_2Eu_6Al_4Se_4Ge_4W_{41}O_{168}(8H_2O)\}^{5-}$ (simulated 2450.4258) and 3095.2129 $\{H_{16}K_6Na_2Eu_6Al_4Se_4Ge_4W_{41}O_{168}(13H_2O)\}^{4-}$ (simulated 3095.3258), respectively (Fig. S17).

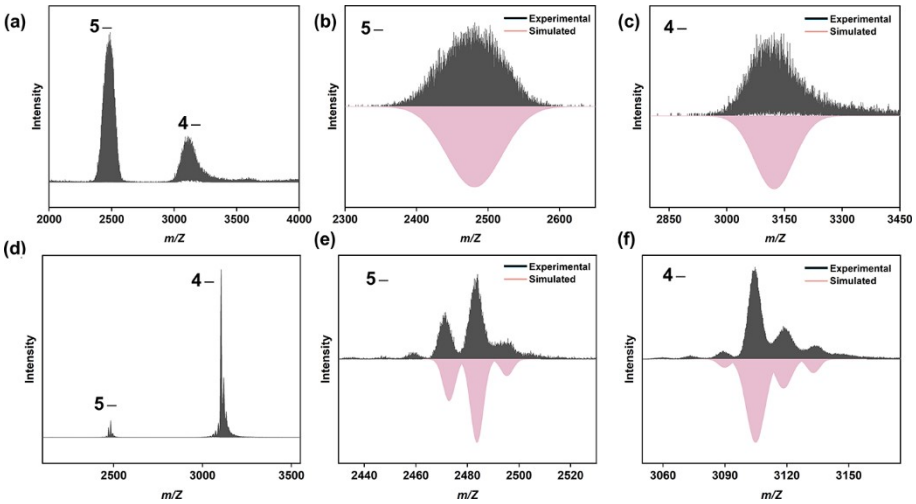

Fig. S22 Experimental (upper, blue) and simulative (under, pink) peaks of the ESI-MS spectra for **1-EuCr**:(a)-(c) in the pH = 3.4 and (d)-(f) in the pH = 10.2.

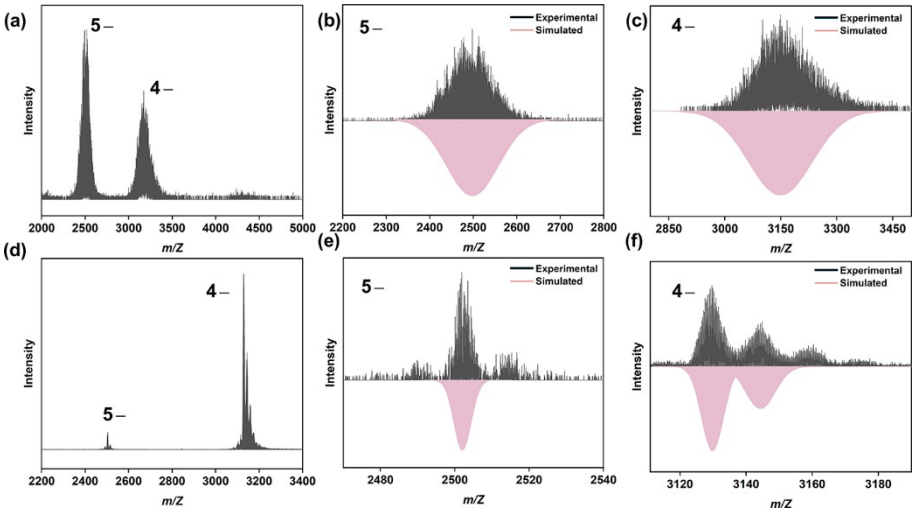

Fig. S23 Experimental (upper, blue) and simulative (under, pink) peaks of the ESI-MS spectra for **2-EuAl**:(a)-(c) in the pH = 3.4 and (d)-(f) in the pH = 10.2

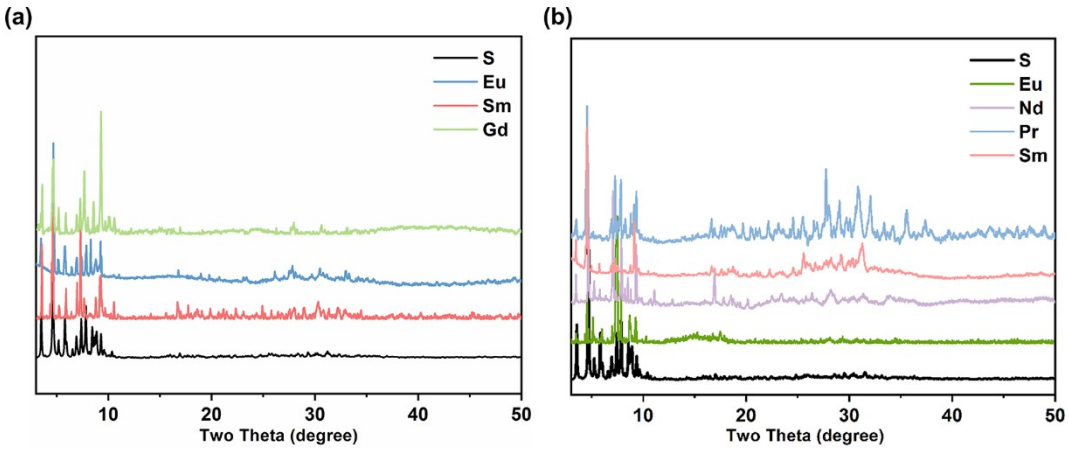

Fig 24. Simulated and experimental PXRD patterns of **1-LnCr** (Ln = Eu, Sm, Gd) (a) and **2-LnAl** (Ln = Eu, Nd, Pr, Sm) (b).

For compound **1-EuCr**, Eu^{3+} can be successfully substituted with Sm^{3+} and Gd^{3+} to yield two iso-structural analogues with **1-EuCr**. For compound **2-EuAl**, Eu^{3+} can be substituted with Nd^{3+}, Pr^{3+}, and Sm^{3+} to afford iso-structural derivatives with **2-EuAl**. XRD measurements confirm that the crystal structures of the substituted are iso-structural and remain unchanged.

References

(1) N. Haraguchi, Y. Okaue, T. Isobe, Y. Matsuda, Stabilization of Tetravalent Cerium upon Coordination of Unsaturated Heteropoly tungstate Anions. *Inorg. Chem.* 1994, **33**, 1015– 1020.